R McAdams et al.

Nonlinear modelling of resistive wall modes using JOREK

Nonlinear modelling of resistive wall modes using JOREK

Rachel McAdams[1,2], IT Chapman[1], M Hoelzl[3], GTA Huijsmans[4], YQ Liu[1], S Pamela[1] and HR Wilson[2]

[1]CCFE, Culham Science Centre, Abingdon, Oxon, OX14 3DB, UK

[2] York Plasma Institute, University of York, Heslington, York, YO10 5DQ, UK

[3] Max Planck Institute for Plasma Physics, Boltzmannstr. 2, 85748 Garching, Germany

[4] ITER Organization, Route de Vinon sur Verdon, 13067 Saint Paul Lez Durance, France

Abstract. The implementation of a resistive wall in the nonlinear MHD code JOREK [M Hoelzl et al, *J. Phys. Conf. Series* **401** 012010 (2012)] has been tested against an analytic theory for the stability of resistive wall modes (RWMs) in cylindrical geometry. For a range of wall positions and wall resistivities, there is good agreement between the calculated linear growth rate of the resistive wall mode in large aspect ratio and that predicted theoretically. Following this successful benchmark of the code, the evolution of resistive wall mode instabilities in a high pressure, high safety factor scenario for ITER has been studied. The RWM growth and behaviour is as expected confirming that the numerical implementation of a resistive wall in JOREK is ready for further exploitation.

1. Introduction and Background

In the steady-state 9MA scenario planned for ITER [1, 2], prolonged plasma operation is facilitated by high pressure and low plasma current leading to high self-generated non-inductive bootstrap current fraction. Furthermore, plasma scenarios considered for next-step fusion reactor designs usually consider plasmas with high plasma pressure to accentuate the non-inductively driven current in order to achieve steady-state plasmas [3, 4, 5]. Indeed, the EU Power Plant Conceptual Study (PPCS) [6] concluded that in order to operate a fusion power plant to produce electricity at economically attractive rates, plasma performance beyond the ITER baseline level [2] is required [7]. However, such plasma parameters make the discharges more susceptible to deleterious magnetohydrodynamic (MHD) instabilities which would not be unstable with conventional H-mode profiles. The ITER steady-state scenario is designed to operate slightly above the no-wall beta limit, meaning that the stability and control of the resistive wall mode (RWM) is a significant concern. Reversed shear discharges have low plasma inductance ($l_i < 0.8$), as the current density peaks off axis, and have predominantly peaked pressure profiles. Both of these facets make such advanced scenarios more prone to kink instabilities manifest as RWMs. The RWM is a macroscopic pressure-driven kink mode, whose stability is mainly determined by damping arising from the relative rotation between the fast rotating plasma and the slowly rotating wall mode. In the absence of a surrounding wall, the plasma is stable to kink modes until the normalised plasma pressure, $\beta = 2\mu_0 \langle p \rangle / B^2$, exceeds a critical value, β_∞. Here $\langle p \rangle$ is the volume averaged plasma pressure and B is the magnetic field. In the presence of an ideally conducting wall, the plasma is stable to a critical value, β_b, with the range $\beta_\infty < \beta < \beta_b$ called the wall-stabilised region. In practice, the vessel wall has a finite resistivity. Thus, on the time scale required for eddy currents to decay resistively, the magnetic perturbation of the external kink mode can penetrate the wall and so wall-stabilisation is lost.

It has been shown in a number of machines that the plasma can in fact operate above the no-wall β-limit [8, 9, 10, 11], even with very low rotation [12, 13, 14]. Whilst the RWM is often treated linearly, there are numerous empirical observations which indicate nonlinear behaviour of the mode interacting with other plasma instabilities [15], energetic particles [16, 17] and plasma rotation [18]. Consequently, in order to make reliable extrapolation to ITER, it is important to understand the nonlinear evolution of the RWM above the predicted no-wall stability limits. The evolution of the RWM has been studied previously analytically [19] and with MARS-Q [20], NIMROD [21] or M3D [22], in each case with different assumptions in the nonlinear models. The JOREK code, a nonlinear MHD code, has been extended to include a resistive wall boundary condition [23] allowing studies, for instance, of the nonlinear evolution of resistive wall modes. The implementation of the resistive wall in JOREK is outlined in section 2, before a benchmarking of this implementation against analytic theory is presented in section 3. Finally, the first nonlinear simulations of resistive wall mode behaviour in

ITER are shown in section 4.

2. Implementation of a resistive wall in JOREK

JOREK is a nonlinear code which solves the reduced MHD equations in toroidal geometry [24, 25]. In the poloidal plane, third order Bézier finite elements are used as the spatial discretisation [26], whereas in the toroidal direction a Fourier decomposition is employed. Thus a 3D model of the plasma can be simulated. A resistive wall model has been implemented [23] for JOREK via a coupling to the STARWALL code such that the interaction of the plasma with 3D conducting structures can be investigated.

2.1. JOREK Equilibrium

JOREK requires the density, temperature and FF' profiles (where $F = RB_\phi$, R is the major radius and B_ϕ is the toroidal magnetic field) and the plasma geometry as input. In addition to minor and major radii, the computational boundary is defined by either the values of the poloidal flux Ψ on the boundary at given (R,Z) coordinates or the ellipticity, triangularities and quadrangularities. After initialisation, JOREK defines the computational boundary and the initial grid for solving the equilibrium. When the flux surfaces have been calculated, the grid is adjusted to align with the flux surfaces.

2.2. Reduced MHD Equations

In the present work, the following reduced MHD model has been used:

- $$\frac{1}{R^2}\frac{\partial \Psi}{\partial t} = \eta(T)\nabla \cdot \left(\frac{1}{R^2}\nabla_\perp \Psi\right) = \frac{1}{R}[u, \Psi] - \frac{F_0}{R^2}\frac{\partial u}{\partial \phi}$$

- $$\hat{\mathbf{e}}_\phi \cdot \nabla \times \left(\rho\frac{\partial \mathbf{v}}{\partial t} = -\rho(\mathbf{v}\cdot\nabla)\mathbf{v} - \nabla(\rho T) + \mathbf{J}\times\mathbf{B} + \mu\Delta\mathbf{v}\right)$$

- $$j = \Delta^*\Psi$$

- $$\omega = \nabla_\perp^2 u$$

- $$\frac{\partial \rho}{\partial t} = -\nabla\cdot(\rho\mathbf{v}) + \nabla\cdot(D_\perp\nabla_\perp\rho) + S_p$$

- $$\rho\frac{\partial T}{\partial t} = -\rho\mathbf{v}\cdot\nabla T - (\kappa-1)\rho T\nabla\cdot\mathbf{v} + \nabla\cdot(K_\perp\nabla_\perp T + K_\parallel\nabla_\parallel T) + S_T$$

where η is the plasma resistivity, T is the plasma temperature, u is the stream function, $\mathbf{v}$ is the velocity, ρ is the density, $\mathbf{J}$ is the current density, $\mathbf{B}$ is the magnetic field, $\Delta^* = R^2\Delta\cdot(R^{-2}\nabla)$, j is the toroidal current density, ω is the vorticity, S_ρ is a density source, κ is the ratio of specific heats, and S_T is a temperature source. K is the transport coefficient, and D is the particle diffusivity. The magnetic field is defined as

$$\mathbf{B} = \frac{F_0}{R}\hat{\mathbf{e}}_\phi + \frac{1}{R}\nabla\Psi\times\hat{\mathbf{e}}_\phi$$

and the flow as

$$\mathbf{v} = -R\nabla u\times\hat{\mathbf{e}}_\phi + v_\parallel\mathbf{B}$$

The weak form of each equation is calculated using test functions equivalent to the JOREK basis functions – Bézier and Fourier basis functions [27] – and any higher derivatives can be reduced by partial integration. The physical quantities are also expanded in the basis functions. The time stepping uses a Crank-Nicholson or Gear's scheme.

2.3. Coupling JOREK and STARWALL

The default boundary conditions in JOREK consist of a computational domain surrounded by an ideally conducting wall. When implementing the free boundary conditions, the boundary integral in the weak form of the current equation remains finite. The STARWALL code [28] solves the magnetic field equation in a vacuum (as a Neumann-like problem). The code can do this in the presence of 3D conducting structures (generally referred to collectively as the "wall") which can include holes, coils and other 3D structures. This allows the inclusion of realistic wall geometry, and modelling MHD stability in machine-specific configurations.

The wall is modelled as infinitesimally thin triangles with the surface currents assumed to be constant within each wall triangle. The wall is also characterised by its effective resistance η_w/d_w where η_w is the wall resistivity (JOREK-normalised) and d_w the wall thickness. STARWALL has previously been coupled to the CASTOR MHD code to perform linear stability studies with a resistive wall [29].

A detailed description of how JOREK is coupled to STARWALL can be found in reference [23]. In the coupling of STARWALL to JOREK, the boundary condition is given by the component of the magnetic field normal to the boundary of the JOREK computational domain in the poloidal plane. This boundary is often referred to as the *interface* [23]. STARWALL generates response matrices for the specified 3D wall structure which can be used to express the magnetic field component tangential to the interface in terms of the normal component.

3. Benchmarking the resistive wall implementation in JOREK

The implementation of the JOREK-STARWALL coupling has previously been benchmarked against the linear MHD code CEDRES++ [30]. In order to validate the $n = 0$ component, the free boundary equilibrium of an ITER-like limiter plasma was computed by JOREK and compared to the same equilibrium computed by CEDRES++. It was found that the results agreed well, with small differences ascribed to the discretisation of the poloidal field coils, as described in reference [23].

Here we demonstrate benchmarking of the resistive wall implementation against an analytical treatment of the Resistive Wall Mode. The growth rate of the ideal kink in a cylindrical plasma of circular cross section, can be calculated analytically [31]. The wall is assumed to be resistive, of thickness d at radius $r_w > a$, where a is the plasma minor radius. The plasma current is a channel, where $\mathbf{J} = J_z\hat{z}$. The step function is

characterised by the parameter r_0 such that

$$J_z(r) = \begin{cases} J_0 & r \leq r_0 \\ 0 & r > r_0 \end{cases} \tag{1}$$

where $r_0 < a$ is the width of the current channel. We also assume zero pressure in the plasma, and a step function for the plasma density with the step located at the same r_0 as the current density profile. From the expression for the current density, the poloidal magnetic field and the safety factor profile can be calculated (with a constant toroidal field $B_z(r) = B_0$). The safety factor is constant at $q_0 = 2B_0/(R\mu_0 J_0)$ within the radius of the current channel, and then increases parabolically to the edge of the plasma.

$$q(r) = \begin{cases} q_0 & r \leq r_0 \\ q_0\frac{r^2}{r_0^2} & r > r_0 \end{cases} \tag{2}$$

Following the calculation found in [31], and assuming modes of the form

$$\psi(r, \theta, z) = \psi(r)\mathrm{e}^{im\theta - inz/R}$$

with m, n the poloidal and toroidal mode numbers respectively, and ψ the perturbed flux. The torque balance equation can be calculated from the z component of the curl of the vorticity equation.

$$\nabla_\perp^2 \psi - \frac{\mu_0 m}{B_\theta(m - nq)}\frac{dJ_z}{dr}\psi = i\gamma\frac{\mu_0 r}{B_\theta(m - nq)}\nabla \times (\rho\mathbf{v}) \cdot \hat{z} \tag{3}$$

where ρ is the plasma density, γ is the growth rate and $\mathbf{v}$ the plasma velocity. Assuming an incompressible, ideal plasma, and using Faraday's law, it is possible to expand the right hand side of Equation 3 to obtain

$$\nabla_\perp^2 \psi - \frac{\mu_0 m}{B_\theta(m - nq)}\frac{dJ_z}{dr}\psi = i\gamma\frac{\mu_0 r}{B_\theta(m - nq)}\rho\nabla_\perp^2\left[\frac{r\psi}{B_\theta(m - nq)} + \frac{d\rho}{dr}\frac{d}{dr}\left(\frac{r\psi}{B_\theta(m - nq)}\right)\right] \tag{4}$$

Equation 4 is reduced to $\nabla_\perp^2\psi = 0$ for $0 \leq r < r_0$ and $r_0 < r \leq a$: this is the vacuum equation for ψ. The jump condition

$$\left.\frac{r\psi'}{\psi}\right|_{r_0} + \frac{2m}{m - nq_0} = (\gamma\tau_A)^2\frac{q_0^2}{(m - nq_0)^2}\left.\frac{r\psi'}{\psi}\right|_{r_0^-} \tag{5}$$

is calculated by integrating Equation 4 across the jump at $r = r_0$, where the Alfven time is $\tau_A = \sqrt{\mu_0\rho_0}R/B_0$, and ρ_0 is the plasma density at the plasma centre.

For a resistive wall located at $r_w > a$, the second jump condition is given by

$$\left.\frac{r\psi'}{\psi}\right|_{r_w} = 2\gamma\tau_w \tag{6}$$

where τ_w is defined as the field penetration time for the m=1 mode, $\tau_w = \mu_0\sigma r_w d/2$, σ is the wall conductivity. Equations 4, 5, and 6 combine to give an equation for the growth rate, γ, of the RWM [31]

$$\frac{\nu}{m - nq_0} - \frac{1}{1 - \frac{\gamma\tau_w}{(\gamma\tau_w + \mu)}\left(\frac{r_0}{r_w}\right)^{2\mu}} = \frac{(\gamma\tau_A)^2}{2}\frac{q_0^2}{(m - nq_0)^2} \tag{7}$$

where $\nu = \mathrm{sgn}(m)$, $\mu = |m|$.

It is possible to neglect the effect of plasma inertia with the ordering $\gamma\tau_A << 1$, $\gamma\tau_w \sim 1$. However, the inertia contribution will be included in the benchmarking. The inertia contribution is essential to capture the behaviour of the plasma when the wall radius is large. Equation 7 is cubic, with one primary root corresponding to the RWM, and two complex conjugate roots to the plasma mode.

In the no-wall limit, $\tau_w = 0$ (or $r_w \to \infty$). The ideal kink should be unstable, which leads to the condition

$$m - \nu < nq_0 < m \tag{8}$$

In the ideal wall limit, $\tau_w \to \infty$, with the wall location at $r = r_w$. The wall radius r_w^{ideal} at which the ideal kink is found to be marginally stable (i.e. $\gamma = 0$) is given by

$$r_w^{ideal} = r_0 \left(1 - \frac{(m - nq_0)}{\nu}\right)^{-\frac{1}{2\mu}} \tag{9}$$

For wall radii $r_w > r_w^{ideal}$, the ideal kink will be unstable. For these radii, the plasma inertia contribution to Equation 7 is necessary.

The toroidal mode number was taken as $n = 1$, and, given that, $m = 2$ was discovered to be the most unstable poloidal mode number for this analytic equilibrium. The plasma equilibrium used in JOREK has a circular cross section, and an aspect ratio $R/a = 10$ to allow comparison to Equation 7, which was derived in a cylindrical plasma. To reproduce the density and current profiles in JOREK, approximations to a step function are used since the discontinuities at $r = r_0$ would be difficult numerically. The level of smoothing employed was tested, but the simulations were found to be insensitive above a threshold.

An individual STARWALL response matrix is required for each of ten wall radii tested from $r_w = 1.1$m to $r_w = 8.0$m. Since $n = 1$ is the most unstable mode, only $n = 1$ modes are included in these linear benchmark simulations. The time taken to establish a linear eigenmode is dependent on the wall radius. In the following results, $q_0 = 1.1$ and the current and density steps are located at $\psi_{N,0} = 0.8$. The marginal wall radius $r_w^{ideal} = 1.59a$ for growth of an ideal kink mode in JOREK is found to agree with Equation 9.

The plasma was surrounded by a resistive wall, with resistivities ranging from $2.5 \times 10^{-1}\Omega$m to $2.5 \times 10^{-6}\Omega$m. The growth rates show the expected behaviour for a RWM as the resistive wall is moved further from the plasma: the stabilising influence of the wall is reduced and the growth rate increases, levelling out as the wall moves to infinity (see figure 1). Additionally, the more conductive the wall, the greater the stabilising influence it exerts on the plasma. The JOREK growth rates can be compared to the calculated growth rates, using Equation 7. A comparison between the analytical and JOREK growth rates can be seen for two different wall resistivities in Figures 1 and 2. The agreement is reasonably good although at the higher wall resistivity there is a slight disagreement when the wall is located close to the plasma edge.

The inertia is important for larger wall radii, where $r_w > r_w^{ideal}$, in which case, equation 7 is cubic in γ. One solution will correspond to the RWM, and the two
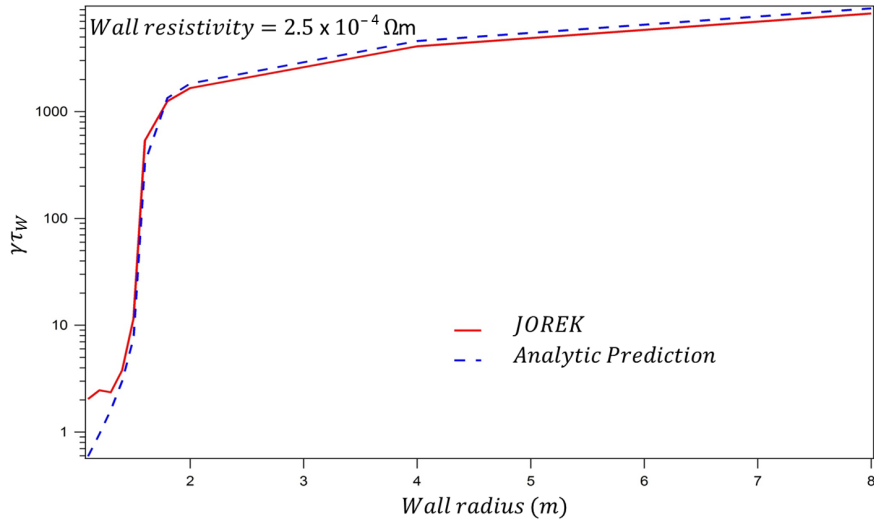
Figure 1. The RWM growth rate as a function of the resistive wall position as predicted by Equation 7 and calculated by JOREK for $\eta_w = 2.5 \times 10^{-4}\Omega m$. At smaller wall radii, JOREK finds larger growth rates than the analytic estimate.
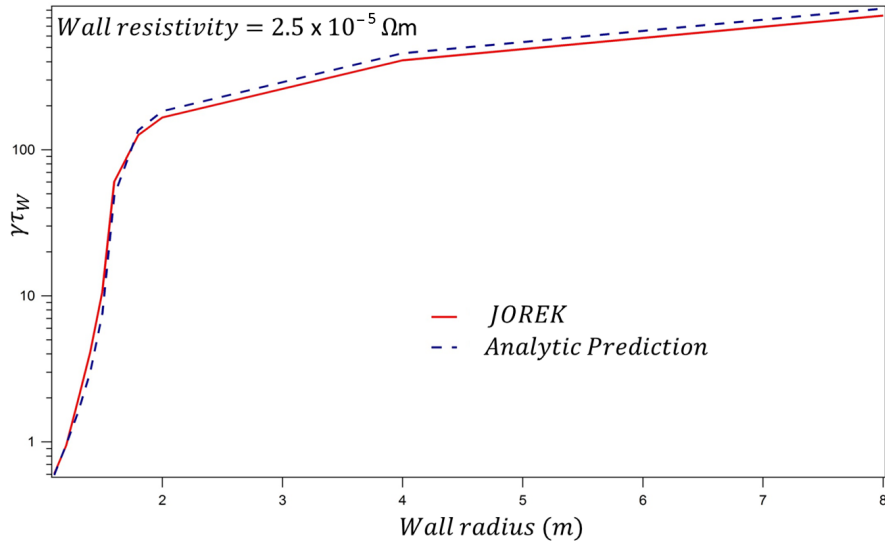

Figure 2. The RWM growth rate as a function of the resistive wall position as predicted by Equation 7 and calculated by JOREK for $\eta_w = 2.5 \times 10^{-5}\Omega m$. The analytic and JOREK simulation growth rates are, for this wall resistivity, very good.

complex conjugate solutions correspond to the plasma mode. Figure 3 shows the results of including the inertia term for a range of wall radii. For wall radii such that $r_w < r_w^{ideal}$, inertia is not a significant contribution to the calculation of the growth rate of the mode. As shown by the dark blue markers, the JOREK growth rate and the analytic calculation excluding the inertia term agree well. For larger wall radii, the dark blue markers showing the analytic growth rate without inertia included disagree substantially
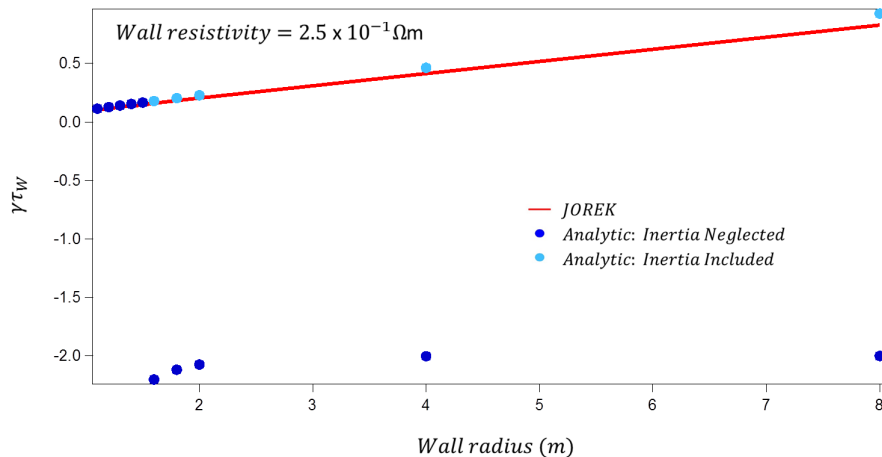
Figure 3. The RWM growth rate as a function of the resistive wall position as predicted by Equation 7 and calculated by JOREK for $\eta_w = 2.5 \times 10^{-1}\Omega m$. The inclusion of the inertia correction into the analytic growth rate equation is crucial for calculating the growth rate for larger wall radii.

with the JOREK results. The inclusion of inertia resolves the discrepancy.

4. ITER simulations with JOREK and realistic wall

Having benchmarked the JOREK-STARWALL coupling against analytic theory for RWM stability, the numerical implementation has been applied to study the resistive wall mode evolution in an ITER advanced scenario plasma, which is expected to experience RWMs at high normalised pressure.

4.1. ITER Equilibrium

The inclusion of the resistive wall is useful while investigating the nonlinear MHD physics in ITER advanced scenarios. The key features that need to be included in the equilibrium are the reversed safety factor profile and a sufficiently high β_N (above the no-wall limit) with a plasma current $I_p = 9\text{MA}$, a toroidal field $B_T = 5.3\text{T}$, a bootstrap fraction $f_{bs} = 0.52$ giving a fusion yield $Q = 5$. Previous simulations of the advanced scenarios for ITER can be found in [32, 33]. The wall is modelled as a thin shell and we consider two cases. The first is an approximation to the ITER first wall, whilst the second is closer-fitting than the ITER first wall. The two wall positions used are shown in Figure 4. A no wall situation can be simulated by setting the wall resistivity very high ($\sim 10^9$).

An equilibrium is constructed with the plasma shape shown in figure 4, a hollow current profile, as shown in figure 5 and the normalised pressure $\beta_N = 2.8$ is above the no-wall limit. This gives rise to a safety factor profile as shown in figure 6. The β_N can be raised by scaling the magnetic field. The linear no-wall pressure limit is found to be
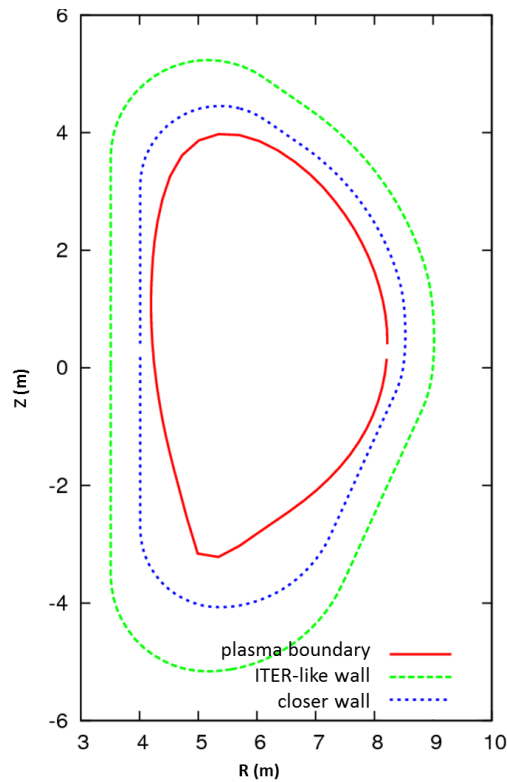
Figure 4. The ITER plasma boundary used in JOREK in R, Z coordinates compared to the two ITER wall positions simulated with STARWALL: one like the wall designed for ITER (dashed) and a second conformal closer-fitting wall (dotted).

$\beta_N^\infty = 2.4$ with $n = 1$ being the most unstable mode. The with-wall limit is found to be $\beta_N^b = 3.4$ in accordance with previous linear stability calculations for a very similar equilibrium [34] using the MISHKA-F code [35].

4.2. Single mode nonlinear stability simulations

After establishing an initial equilibrium with suitable parameters, it can be evolved in time. It is necessary to include finite profiles for the plasma resistivity and viscosity in order to avoid numerical instability. Without dissipation in the plasma, small scale structures which may develop cannot be resolved by the code. Dissipation will limit how fine these structures become. This allows further evolution, through a linear phase to saturation of the mode. The mode found is a global mode, with a displacement across the whole poloidal cross section.

Figure 7 shows the mode in the saturation phase, for $\beta_N = 2.6$ and plasma resistivity $\eta_p = 2.6 \times 10^{-6}$ (this is given in JOREK-normalised units, which are given by $\eta_{SI} = \eta_{JOREK} \sqrt{\mu_0/\rho_0}$ where ρ_0 is the central density of the plasma). The plots show the $n = 1$ flux perturbation to the equilibrium plasma in the poloidal cross section. The three plots show the mode with an ITER-like wall (with the corresponding real value of
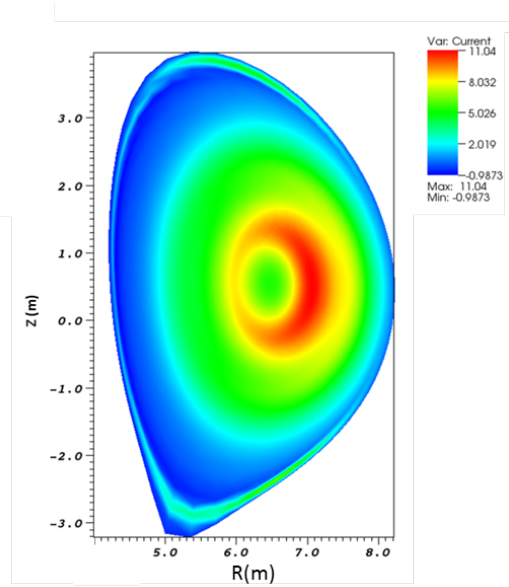
Figure 5. The poloidal cross section of the plasma current density showing the hollow current profile necessary for a reversed shear q profile.
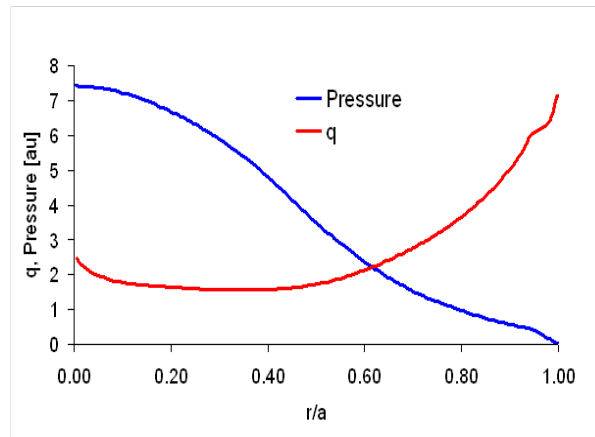

Figure 6. The ITER advanced scenario q-profile and pressure profile as a function of the normalised toroidal flux.

the ITER wall resistivity), the second, more closely-fitting wall (of the same resistivity as the ITER-like wall), and an ideal wall at the plasma separatrix. Moving the wall closer to the plasma partially stabilises the mode: the saturated nonlinear perturbation amplitude is smaller and the poloidal cross sections show that although the displacement has a similar structure, it has been reduced by the closer-fitting wall. Comparison with the mode when an ideal wall is placed at the ITER wall location shows that the ideal wall stabilises the global mode, with more localised perturbations. These structures at the top and bottom of the plasma shown in Figure 7 for the ideal wall on the separatrix
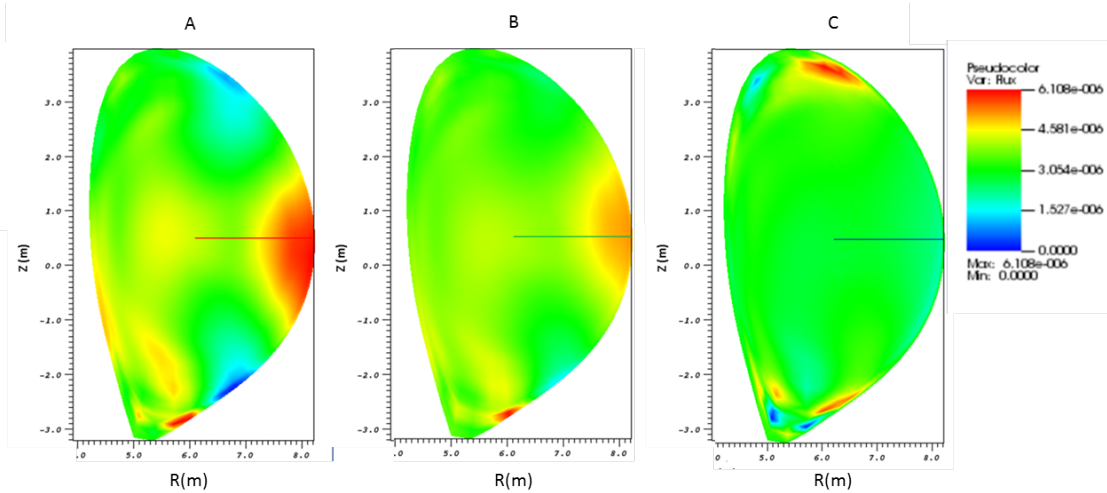
Figure 7. Comparison of the poloidal cross-section of the saturated modes for $\beta_N = 2.6$ and different wall configurations A, B, and C: ITER-like wall, closely-fitting wall and ideal wall on the separatrix, respectively. Plots A and B have the same wall resistivity. The poloidal plots show the $n = 1$ flux perturbation. Moving the wall closer to the plasma partially stabilises the mode, whilst the ideal wall seems to stabilise global perturbations.

are also seen in the linear phase of growth of the RWM in cases with sufficient plasma resistivity, as discussed in the next section.

4.2.1. Effect of plasma resistivity   Although the RWM is not a resistive instability and its growth rate should not depend on the plasma resistivity, the inclusion of plasma resistivity to avoid numerical problems associated with insufficient dissipation has been investigated in order to find whether it affects the simulation results. The plasma resistivity has been scanned while keeping $\beta_N = 2.6$ and using the ITER-like wall as the boundary condition. Previous simulations were carried out at a plasma resistivity $\eta_p = 2 \times 10^{-6}$ (in JOREK units). For plasma resistivities less than $\sim \eta_p = 1.4 \times 10^{-7}$, the plasma is stable, and the energy only oscillates instead of entering the linear growth phase. For plasma resistivities greater than this value, the plasma is unstable and the mode is able to grow. Figure 8 shows the growth rates for the simulations which vary plasma resistivity. It can be seen that for small plasma resistivities, the growth rate is negative: increasing the plasma resistivity increases the growth rate. For sufficiently large plasma resistivity, the RWM grows. This may be explained by the Glasser-Greene-Johnson [36] effect as the RWM couples to tearing layer damping [37].

4.2.2. Effect of plasma pressure   The mode stability has been explored by changing β_N, and keeping the ITER-like wall as the boundary condition. Increasing β_N would be expected to increase the mode growth rate, since it corresponds to increasing the plasma pressure. The β_N has been varied by scaling the magnetic field and simultaneously altering the plasma pressure profile in order to retain a constant minimum safety factor
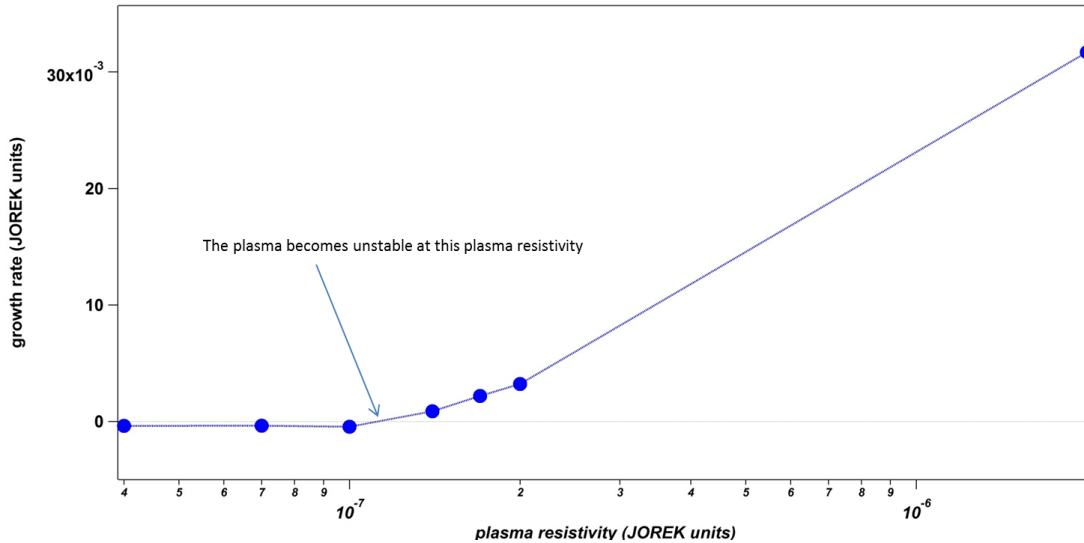
Figure 8. The plot shows the growth rates for the different values of plasma resistivity for $\beta_N = 2.5$, with the ITER-like wall included. The marginal stability point can be seen when the growth rates become positive.

profile. Figure 9 shows the JOREK growth rate for a range of β_N with the same boundary condition of the ITER-like wall. As expected, an increase in β_N corresponds to an increase in the growth rate of the mode.

4.2.3. Effect of wall resistivity The effect of changing the wall resistivity on the RWM growth rate has also been studied. Figure 10 shows that for an ITER advanced tokamak plasma with plasma resistivity fixed at $\eta_p = 2 \times 10^7$ (in JOREK units) and $\beta_N = 2.7$, the RWM growth rate decreases for an increasingly ideal wall, as expected. As the wall tends to the ideal wall limit at very low η_W the RWM is stabilised, but as the wall resistivity increases, the growth rate increases and tends towards the no-wall limit.

4.3. Multiple mode nonlinear stability simulations

Recently there have been observations of RWM coupling with core plasma instabilities [16, 38, 17] and edge localised modes [17], illustrating the importance of understanding the nonlinear interaction of RWMs with other modes [19]. Initial calculations for MAST plasmas have shown that the growth of an $n = 1$ RWM can lead to the destabilisation of core tearing modes due to perturbations in the current profile [39]. Similarly, JOREK has been used to study the nonlinear excitation of low-n modes by higher-n instabilities in simulations of edge localised modes [40]. Following the benchmarking of the resistive wall implementation in JOREK presented in Section 3, the nonlinear evolution of the RWM has been studied in an ITER advanced scenario plasma. Here we consider an ITER plasma with a plasma resistivity $\eta_p = 2 \times 10^{-7}$ (in JOREK units), a wall resistivity
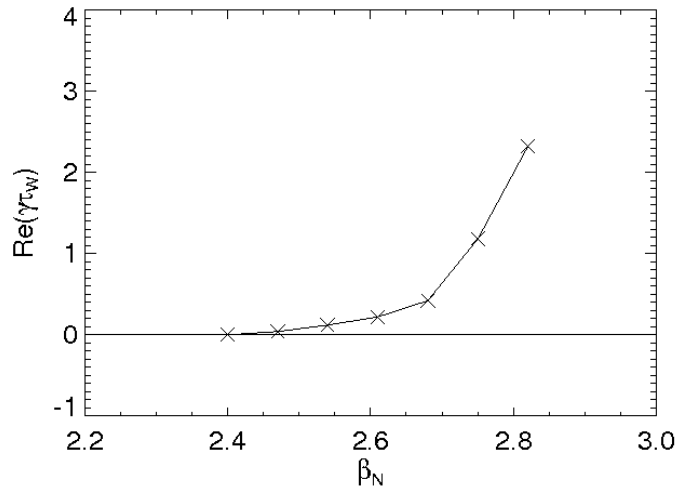
Figure 9. The RWM growth rate as a function of β_N for the ITER advanced scenario with the resistive ITER-like wall, and at the marginal plasma resistivity of 1.4×10^{-7}. The β scan is carried out by adjusting B_ϕ and the plasma pressure in order to keep the minimum safety factor constant but change β_N. As would be expected, increasing β_N increases the growth rate of the mode.

$\eta_W = 1 \times 10^{-4}$, a normalised pressure $\beta_N = 2.6$ and simulate multiple modes $n = 1 - 5$ nonlinearly. For these plasma parameters marginally above the no-wall limit, the $n = 1$ mode is found be the most unstable. From figure 11 it is evident that whilst the $n = 1$ mode has the highest initial linear growth rate, the higher-n modes grow more rapidly at later times and there is a nonlinear coupling between the different modes. Capturing this nonlinear interaction is important when assessing the stability limits for advanced scenario plasmas in steady-state conditions.

5. Discussion and conclusions

The implementation of the resistive wall in JOREK has been successfully benchmarked against an analytic theory for the stability of the resistive wall mode in cylindrical geometry. The inclusion of the resistive wall is achieved by coupling JOREK to STARWALL. By using a linear model for a RWM, the growth rates found in JOREK simulations could be compared against calculated rates. JOREK finds the same wall radius at which an ideal wall would stabilise the ideal kink as the analytic theory. There was also good agreement when the wall was resistive. The wall resistivity is found to affect the quantitative agreement, though the qualitative behaviour is always in good accordance.

JOREK was then used to simulate advanced tokamak plasmas in an ITER geometry. Coupled to STARWALL, the wall is modelled as the realistic ITER first wall with the corresponding resistivity. A plasma equilibrium was constructed which is unstable to a
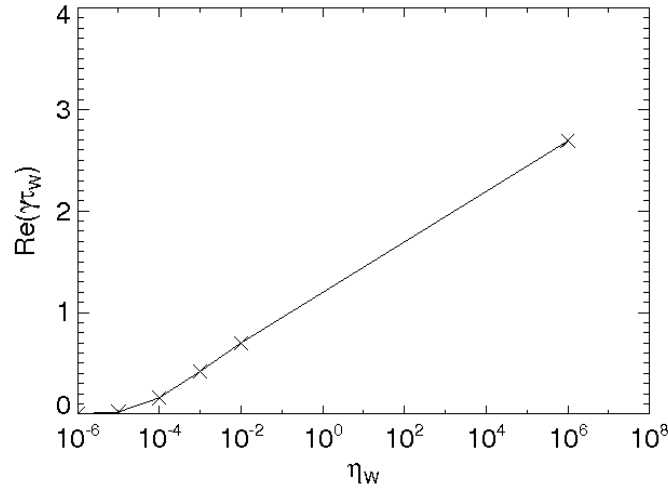
Figure 10. The RWM growth rate as a function of wall resistivity for the ITER advanced scenario with an ITER-like wall, and at the marginal plasma resistivity of 2×10^{-7} and $\beta_N = 2.7$. As the wall tends to ideal at very low resistivity, the kink mode is stabilised, but for the effective no-wall case with very high resistivity, the kink mode is unstable as the plasma is at a pressure above the no-wall limit, $\beta_N^\infty = 2.5$.
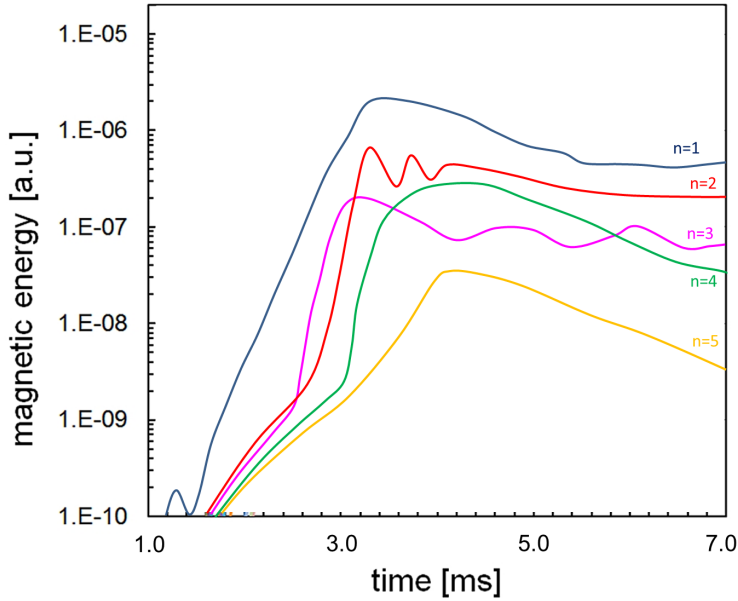

Figure 11. The magnetic energy of the $n = 1-5$ modes in an ITER advanced tokamak plasma with a resistive wall with plasma resistivity $\eta_p = 2 \times 10^{-7}$, a wall resistivity $\eta_W = 1 \times 10^{-4}$, a normalised pressure $\beta_N = 2.6$. There is a nonlinear interaction between the linearly most unstable mode, $n = 1$ and the high-n modes which become more unstable during the growth of the $n = 1$ mode.

Resistive Wall Mode. The effects of changing the plasma resistivity, the plasma pressure and the wall resistivity have been studied and behave as expected theoretically.

The successful comparison of the resistive wall implementation in JOREK to analytic theory and initial simulations of ITER provide a platform for further studies of the nonlinear evolution of RWM stability in advanced tokamak scenarios. Initial simulations show the importance of nonlinear evolution of the RWM since higher-n modes are stimulated during the linear growth phase of the $n = 1$ kink mode, which is found to be the most unstable linearly. Understanding and accounting for this nonlinear evolution will be important when assessing the stability limits in advanced tokamak plasmas in view of both operating the steady-state $Q = 5$ scenario in ITER and longer term for design of fusion power plant plasmas.

[1] A Polevoi et al 2002 *Proc 19th Int Conf on Fusion Energy 2002* (Lyon, France) Vienna:IAEA
[2] ITER Physics Basis 2007 *Nucl. Fusion* **47** S1
[3] CE Kessel, TK Mau, SC Jardin and F Najmabadi, Fus. Eng. Design, 80 (2006) 63
[4] SC Jardin et al, Fus. Eng. Des., 80 (2006) 25
[5] YR LinLiu and RD Stambaugh, Nucl. Fusion, 44 (2004) 548
[6] D Maisonnier et al, Fus. Eng. Design, 81 (2006) 1123
[7] DJ Campbell et al, 21st IAEA Fusion Energy Conference, Chengdu (2006) FT/1-1
[8] Strait EJ *et al* 1995 *Phys. Rev. Lett.* **74** 2483
[9] Hender TC *et al* 2006 *21st IAEA Fusion Energy Conference, Chengdu, China* **EX/P8-18**
[10] Sabbagh SA *et al* 2006 *Nucl. Fusion* **46** 635
[11] Garofalo AM *et al* 2002 *Phys. Plasmas* **9** 1997
[12] Reimerdes H *et al* 2007 *Phys. Rev. Lett.* **98** 055001
[13] Takechi M *et al* 2007 *Phys. Rev. Lett.* **98** 055002
[14] Sabbagh SA *et al* 2010 *Nucl. Fusion* **50** 025020
[15] G. Matsunaga, N. Aiba, K. Shinohara, Y. Sakamoto, M. Takechi, T. Suzuki, N. Asakura, A. Isayama, N. Oyama, and JT-60 Team, "Interactions between MHD instabilities in the wall-stabilized high-beta plasmas" *Proc 23rd IAEA Fusion Energy Conference, Daejon, Korea Rep* EXS/5-3 (2010)
[16] G. Matsunaga, K. Shinohara, N. Aiba, Y. Sakamoto, A. Isayama, N. Asakura, T. Suzuki, M. Takechi, N. Oyama, H. Urano and the JT-60 Team, *Nucl. Fusion* **50** 084003 (2010)
[17] M. Okabayashi, G. Matsunaga, M. Takechi, J.S. deGrassie, W.W. Heidbrink, Y. In, Y.Q. Liu, E.J. Strait, N. Asakiura, R. Budny, G, Jackson, J. Hanso n, R.J. La Haye, M.J. Lanctot, J.Manickam, H. Reimerdes, and K. Shinohara, *Phys. Plasmas* **18** 056112 (2011)
[18] H. Reimerdes, A.M. Garofalo, E.J. Strait, R.J. Buttery, M.S. Chu, G.L. Jackson, R.J. LaHaye,

M.J. Lanctot, Y.Q. Liu, J.-K. Park, M. Okabayashi, M. S chaffer, and W. Solomon *Nucl. Fusion* **49** 115001 (2009)

[19] R McAdams, HR Wilson and IT Chapman, *Nuclear Fusion* **53** 083005 (2013)

[20] YQ Liu and Y Sun *Phys Plasmas* **20** 022505 (2013)

[21] AL Becerra et al, "Studies of NSTX equilibria with beta above the n=1 no-wall limit using new toroidal resistive wall boundary condition in NIMROD" *Proc APS Division of Plasma Physics Meeting, New Orleans, USA* BP8.00047 (2014)

[22] H Strauss et al, *Proceedings of the 20th IAEA Fusion Energy Conference (Vilamoura, Portugal)* TH/2-2 (2004)

[23] M. Hoelzl, P. Merkel, G. T. A. Huysmans, E. Nardon, E. Strumberger, R. McAdams, I. T. Chapman, S. Guenter, and K. Lackner. *J. Phys. Conf. Ser.* **401** 012010 (2012)

[24] G. T. A Huysmans and O. Czarny. *Nucl. Fusion* **7** 659 (2007)

[25] G. T. A. Huysmans, S. Pamela, E. van der Plas, and P Ramet. *Plasma Phys. Cont. Fusion* **12** 124012 (2009)

[26] O. Czarny and G. T. A. Huysmans *J. Comp. Phys.* **16** 7423 (2008)

[27] C. Hirsch. Numerical computation of internal and external ows., volume 1. J.Wiley. ISBN 09780471924524

[28] P. Merkel and M. Sempf. "Feedback stabilization of resistive wall modes in the presence of multiply connected wall structures" *Proceedings of the 38th EPS Conference On Plasma Physics (Strasbourg, France)* P5.082 (2006)

[29] E. Strumberger, P. Merkel, C. Tichmann, and S. Guenter. "Linear stability studies in the presence of 3D wall structures" *Proceedings of the 21st IAEA Fusion Energy Conference (Chengdu, China)* TH/P3-8 (2006)

[30] P. Hertout, C. Boulbe, E. Nardon, J. Blum, S. Bremond, J. Bucalossi, B. Faugeras, V. Grandgirard, and P. Moreau. "The CEDRES++ equilibrium code and its application to ITER, JT-60SA and Tore Supra" *Fusion Engineering and Design: Proceedings of the 26th Symposium of Fusion Technology (SOFT-26)* **86** 1045 (2011)

[31] Yueqiang Liu, R. Albanese, A. Portone, G. Rubinacci, and F. Villone *Phys. Plasmas* **15** 072516 (2008)

[32] A. R. Polevoi et al. *J. Plasma Fusion Res. SERIES* **5** 82 (2002)

[33] S. H. Kim et al. "CORSICA simulations of ITER advanced operation scenarios" *Proc. 39th EPS Conf. Stockholm, Sweden* P5.089 (2012)

[34] IT Chapman et al, *Physics of Plasmas* **19** 052502 (2012)

[35] IT Chapman et al, *Physics of Plasmas* **13** 062511 (2006)

[36] AH Glasser, JM Greene, and JL Johnson, *Phys. Fluids* **18** 875 (1975)

[37] He et al, *Phys Rev Lett* **113** 175001 (2014)

[38] Matsunaga G et al. 2009 *Phys Rev Lett* **103** 045001

[39] IT Chapman et al *Nuclear Fusion* **51** 073040 (2011)

[40] I Krebs, M Hoelzl, K Lackner and S Guenter *Phys Plasmas* **20** 082506 (2013)